Solar-Terrestrial Physics. 2026, vol. 12, iss. 2, pp. 114–118. DOI: 10.12737/stp-121202613. © 2026 M.V. Globa, A.V. Gubin, S.V. Lesovoi. Published by INFRA-M Academic Publishing House

DOI: 10.12737/stp-121202613
EDN: PGMHSR

Received November 07, 2025
Accepted March 02, 2026

CORRECTION FOR POINTING ERRORS OF SIBERIAN RADIOHELIOGRAPH ANTENNAS

M.V. Globa
Institute of Solar-Terrestrial Physics SB RAS, Irkutsk, Russia, globa@iszf.irk.ru

A.V. Gubin
Institute of Solar-Terrestrial Physics SB RAS Irkutsk, Russia, lgubin@mail.ru

S.V. Lesovoi
Institute of Solar-Terrestrial Physics SB RAS, Irkutsk, Russia, svlesovoi@gmail.com

Abstract. For radio interferometers, antenna pointing accuracy is critical, as deviations in the direction of the beam from the source not only reduce the signal level, but also lead to incorrect measurements of visibility phases. These distortions cannot be corrected during data processing and reduce the dynamic range of images. The measurement method involves determining the deviation of the beam from the center of the Sun for different azimuth and elevation angles and fitting the resulting dependence using a model developed for altazimuth mounts. The model allows us to determine the deviation of the mount axis from the zenith direction, the non-orthogonality of the azimuth and elevation axes, the azimuth offset of the feed, and the azimuth and elevation constants. Mechanical adjustment of these parameters with the specified accuracy is impossible, so the correction was performed by introducing corrections to each moment in time for each antenna. Using the described technique, we managed to achieve an antenna pointing accuracy of approximately 2 arcmin.

Keywords: solar radio telescope, pointing of altazimuth mounts.

INTRODUCTION

Measuring and correcting the antenna pointing accuracy is one of the key steps in adjusting radio telescope equipment. The antenna pointing accuracy directly affects the quality and fidelity of images obtained by aperture synthesis. If an accuracy of 1/10 of the antenna beamwidth is considered acceptable for a single antenna, the requirements for synthesizing telescopes are even higher, since inaccurate pointing leads to incorrect measurement of visibility and hence to image distortions. For example, with a pointing error of 10 arcmin, the error in determining the visibility phase corresponding to the shortest antenna baselines will be 10°. This is by an order of magnitude beyond the accuracy of phase measurement required to achieve the 40 dB dynamic range of images, which is needed for observing solar flares. In other words, pointing errors of individual antennas lead to the fact that the measured visibility and the true brightness angle distribution are no longer related by the Fourier transform [Thompson et al., 2003], hence the image fidelity decreases.

SRH ANTENNAS

The Siberian Radioheliograph (SRH) consists of three T-shaped antenna arrays operating in frequency ranges 3–6, 6–12, and 12–24 GHz and receiving both circular polarizations (right/left circular polarization, RCP/LCP) [Altyntsev et al., 2020]. SRH antennas are straight-focus parabolic reflectors mounted on altazimuth mounts (Figure 1). Parameters of the SRH antennas are listed in Table 1. At SRH, the correction technique based on response analysis has been tested for the first time, since the previous instruments (SRH-48, SRH-10, and SSRT) used mounts of another type and the control system did not allow individual corrections to be made for each antenna. The SRH antennas are controlled by uploading a table of coordinates, calculated at an interval of 1 s, into the control unit of each antenna, after which the antenna moves autonomously according to this table. The tables are calculated taking into account atmospheric refraction [Holleman, Huuskonen, 2003].

MEASUREMENT TECHNIQUE

For altazimuthal antenna mounts employed in radio astronomy, a technique has been developed to identify mount parameters, which have an effect on antenna pointing, by analyzing measured deviations of the beam from the direction to a known radio astronomy object for different azimuth and elevation angles [de Vicente, Barcia, 2007; Mangum, 2001; Sun et al., 2019]. The model is presented as follows:

$$\Delta A = P_1 + P_2 \sec h + P_3 \tan h + \\ + P_4 \tan h \cos A + P_5 \tan h \sin A, \quad (1)$$

$$\Delta h = P_7 - P_4 \sin A - P_5 \cos A + \\ + P_8 \sin h + P_9 \cos h, \quad (2)$$

where A, h are azimuth and elevation respectively; ΔA, Δh are azimuth and elevation errors; mount parameters P_i are presented in Table 2.

Figure 1. Antenna of SRH 3–6 GHz array

The parameter P_6 — the elevation offset of the feed — is omitted from the model, since it has a constant elevation error and is indistinguishable from P_7. Gravitational effects are ignored due to the low mass of mirrors. When estimating pointing errors, several sources are generally selected in different parts of the celestial sphere and are tracked by periodically measuring the deviation of the beam. The measured mount parameters may then be used either to calculate corrections to source coordinates or for physical adjustment if mount and feed designs allow. For SRH, the only object of observation is the Sun due to the small collecting area of individual antennas. This places restrictions on the range of angles for which pointing errors can be estimated, so the parameters measured by the model may not fully match the physical parameters of the mount. Nevertheless, the calculated corrections to the coordinates will be valid, since they are measured for the part of the celestial sphere in which the observation is conducted.

Pointing errors were estimated near the summer solstice to cover the largest range of azimuth and elevation changes. During the observation day, the antennas were pointed away from the Sun's center in azimuth and elevation every 10 min and deviations of the beam from the direction to the Sun's center ΔA, Δh were measured for each antenna. The daily deviation behavior for antenna E3040 is indicated in the left panel of Figure 2 by colored lines, and black lines show the result of fitting by the model described above. Based on the obtained model parameters, individual antenna pointing tables have been compiled for each antenna — at each moment in time, an appropriate correction is added to the coordinates of the Sun's center. To evaluate the result, control measurements were carried out in the same way (with antennas pointing away from the Sun's center every 10 min throughout the observation day). The result for antenna E3040 is presented on the right in Figure 2. The error spread for all antennas of the 3–6 GHz array before and after correction is shown in Figure 3. We managed to reduce the spread from 6 to 2 arcmin.

RESULTS AND DISCUSSION

Unlike the routine mode when monitoring is conducted at 16 frequencies with ~3.5 s resolution, when checking the antenna pointing, SRH operated in the three-frequency mode to increase the time resolution and improve the accuracy of determining beam deviations. Thus, we obtained data on antenna pointing for each array at lower, central, and upper frequencies of the corresponding range in two circular polarizations. Figure 4 illustrates the spread of beam directions in different polarizations. In the 3–6 and 6–12 GHz arrays, there is an offset of beam at the upper frequency (5.6 and 11.8 GHz respectively) mainly

Table 1

Parameters of SRH antennas

Parameter	SRH 3–6 GHz	SRH 6–12 GHz	SRH 12–24 GHz
Number of antennas	127	192	207
Antenna diameter, m	3	2	1
f/D	0.4	0.4	0.8
Beamwidth, deg.	2–1	1.6–0.8	1.6–0.8

Table 2

Mount parameters determined by the pointing model

P_1	Azimuth encoder error. Positive value corresponds to larger azimuths
P_2	Azimuth offset of the feed. Positive value corresponds to larger azimuths
P_3	Nonorthogonality between azimuth and elevation axes
P_4	Deviation of the mount azimuth axis in the east–west direction. Positive value corresponds to an eastward deviation
P_5	Deviation of the mount azimuth axis in the north–south direction. Positive value corresponds to a southward deviation
P_7	Elevation encoder error. Positive value corresponds to high elevations
P_8, P_9	Gravitational effect

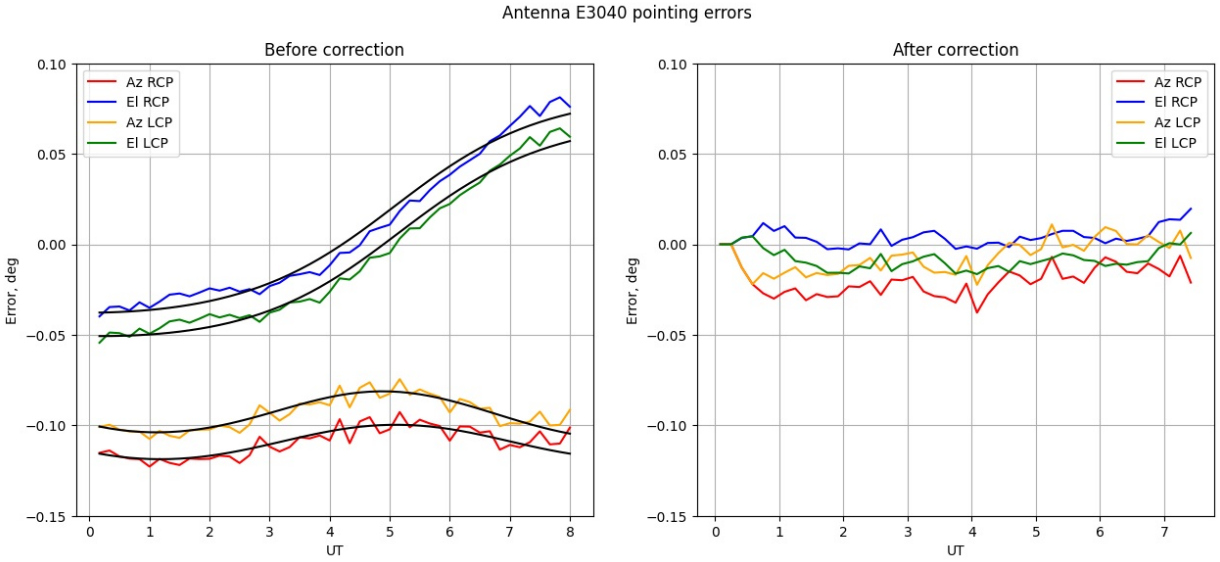

Figure 2. Pointing errors of antenna E3040 before (on the left) and after (on the right) correction of mount parameters. Along the Y-axis are azimuth and elevation in degrees. Black lines in the left panel indicate the result of fitting. The correction was performed by calculating individual antenna pointing tables for each antenna

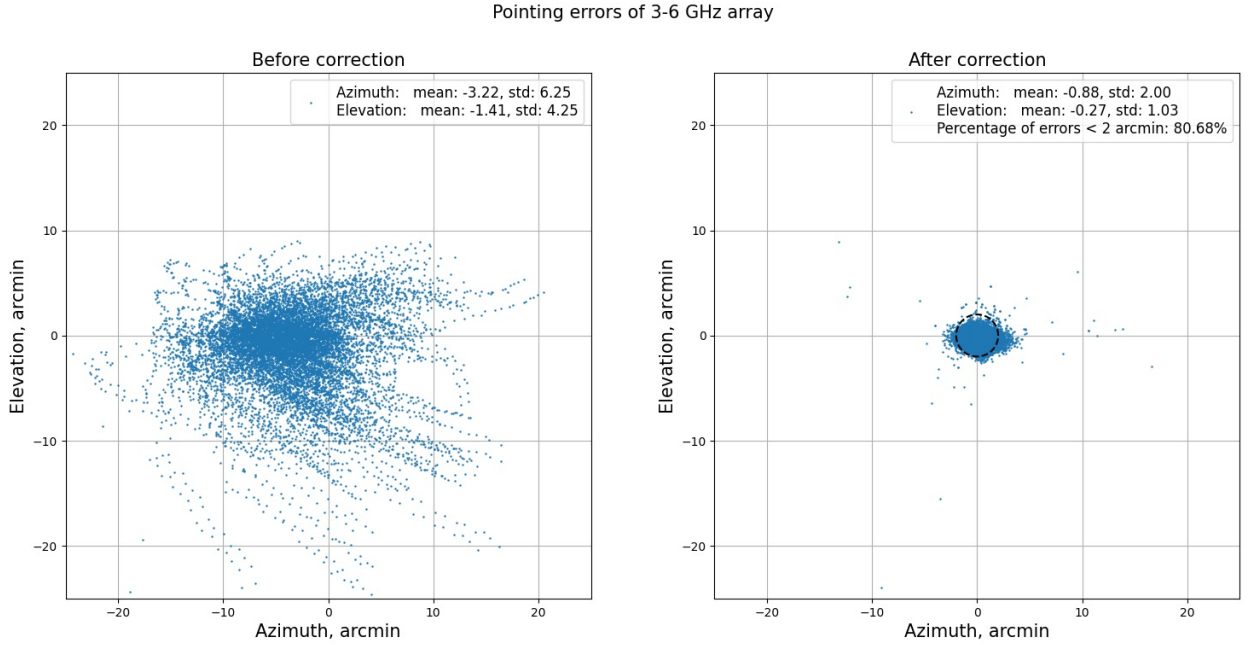

Figure 3. Pointing errors of all antennas of the 3–6 GHz array for the entire measurement day in both circular polarizations at a frequency of 3 GHz: on the left — before correction, on the right — after correction; statistical parameters of each distribution are shown at the top. In the right panel, black dashes depict a circle of 2 arcmin radius within which 80 % of all deviations fall

mainly in azimuth by ~3 arcmin. There is no such an offset in the 12–24 GHz array, since the highest measurement frequency is 20 GHz, whereas in the routine mode observations are made at frequencies out to 23.4 GHz. This choice of frequencies is due to the fact that the signal at frequencies above 20 GHz is affected by noise. Figure 5 illustrates the spread of beam directions at different frequencies. It is apparent that at low and medium frequencies of each range the differences do not exceed 2 arcmin for most antennas either. More significant deviations are observed only at the upper frequency of the 3–6 and 6–12 GHz ranges. We can conclude that the difference in the direction of the beam in different polarizations for the vast majority of SRH antennas does not exceed 2 arcmin in most of the range.

Inaccuracies in pointing SRH antennas give rise to non-factorable phase errors in measuring visibility, which are not eliminated through calibration of antenna gains. The cause of such errors is that antenna pointing inaccuracies introduce an asymmetry into the response of a two-element interferometer. To evaluate the effect of pointing errors on a resulting image, we examine the formation of

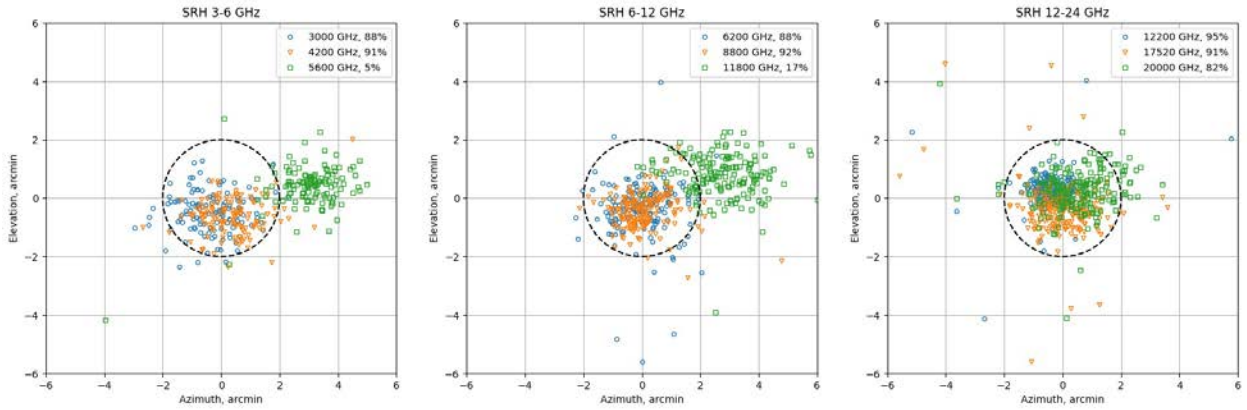

Figure 4. Difference in the direction of antenna beam in two polarizations for three SRH arrays. Each symbol represents a specific antenna and indicates how the beam will deviate in the left polarization if it is directed to the origin in the right one. Frequencies are highlighted in color; the percentage is given of points located inside the circle of 2 arcmin radius (black dashes)

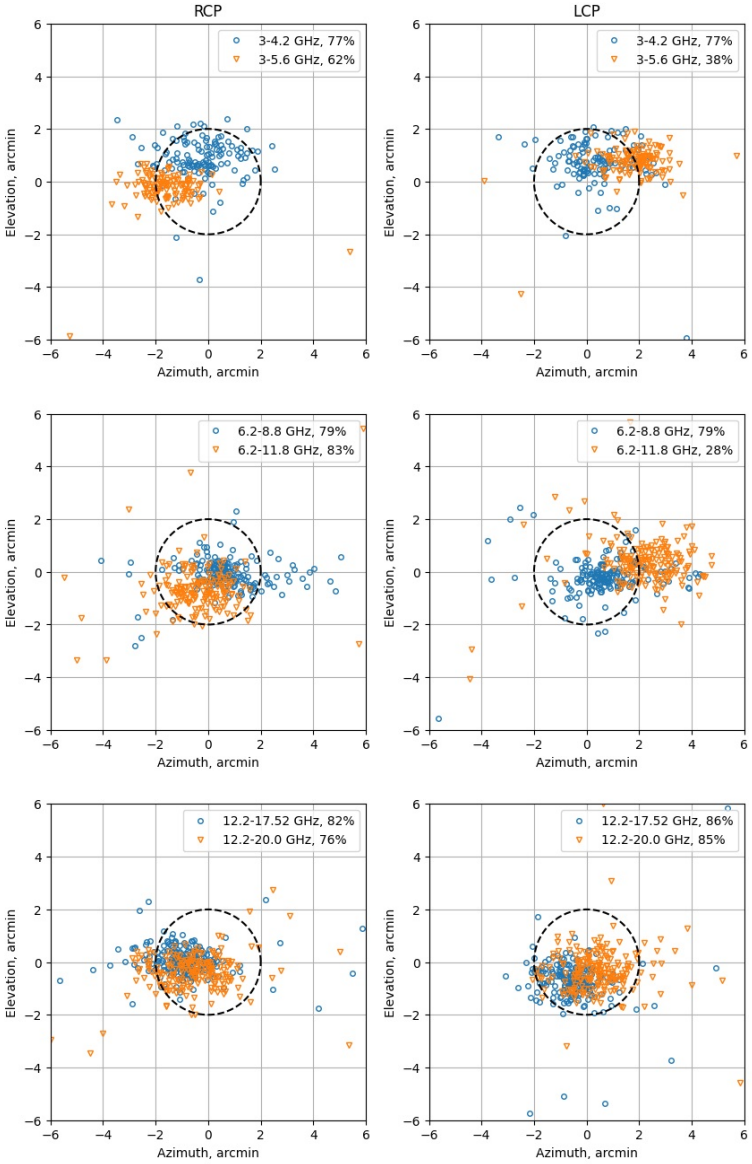

Figure 5. Difference in the direction of the antenna beam at different frequencies for the right (left) and left (right) polarizations: in upper panels is the array 3–6 GHz; in middle panels, 6–12 GHz; and in lower ones, 12–24 GHz. Each symbol denotes one antenna and indicates how the beam will deviate at medium (blue) or upper (orange) frequency if it is directed to the origin at the lower frequency of the range. In the top right corner of each panel is the percentage of points located inside the circle of 2 arcmin radius (black dashes)

the response of the two-element interferometer in terms of deviations in pointing. Designate analytical signals at outputs of the antennas k, l as Z_k, Z_l. Then, the real part of the measured visibility is

$$\mathrm{Re}\left\langle Z_k\, Z_l^*\right\rangle_t = \left\langle \int_{4\pi} A_k(\theta) E_k(\theta, t)\, d\theta \times \right. \\ \left. \times \int_{4\pi} A_l(\theta) E_l(\theta, t)\, d\theta \cos\left(2\pi u\, \theta\right)\right\rangle_t, \quad (3)$$

where θ is the angle in radians; E is the angle distribution of radio brightness; A is the antenna pattern; $u = b_{kl}/\lambda$ is the spatial frequency corresponding to the antenna baseline and operating wavelength. Taking into account the ergodicity $E(\theta, t)$ (physically this means that the angle distribution of radio brightness is spatially incoherent, and the sampling frequency exceeds twice the operating frequency range), Expression (3) can be represented as

$$\mathrm{Re}\left\langle Z_k\, Z_l^*\right\rangle_t = \int A_k(\theta) A_l(\theta) I(\theta) \cos\left(2\pi u \theta\right) d\theta, \quad (4)$$

where $I = \left\langle E_k\, E_l^*\right\rangle_t$ is the intensity angle distribution. A similar expression can be derived for the imaginary part of the measured visibility:

$$\mathrm{Im}\left\langle Z_k\, Z_l^*\right\rangle_t = \\ = \int A_k(\theta) A_l(\theta) I(\theta) \sin\left(2\pi u\, \theta\right) d\theta. \quad (5)$$

Suppose that $I(\theta)$ is a symmetric function. Then, the phase of the measured visibility should be equal to 0. If the antenna pointing errors $\Delta\theta_k$, $\Delta\theta_l$ do not compensate each other, the expression $A_k(\theta+\delta\theta_k)A_l(\theta+\delta\theta_l)$ will be asymmetric and a phase error will arise in the measured visibility. Since antenna patterns are included in the expression under integral sign, this error is not factorable — it cannot be represented by a pair of multipliers depending on antenna number. Such errors affect the results of calibration of antenna gains and the resulting image. Quantitatively, the effect of these errors can be described in terms of the dynamic range of the image [Perley, 1999] $D \approx N/\Delta\varphi$, where N is the number of radio interferometer antennas; $\Delta\varphi$ is the phase noise of measured visibility. Modeling (4) and (5) has revealed that the phase error $\Delta\varphi$ in the visibility of five shortest antenna baselines, used for calibration, with – pointing error of 2 arcmin will vary from 2° to 10°. Such phase errors will limit the dynamic range of images to ~30–35 dB.

CONCLUSION

The paper has described a method of measuring pointing errors of SRH antennas and rectifying them by correcting coordinates for each antenna. Due to the correction, we managed to significantly improve the antenna pointing accuracy and hence the quality and fidelity of the data obtained. Taking into account the spread of beam directions at different frequencies and in different polarizations, we can conclude that 2 arcmin is the maximum achievable antenna pointing accuracy for SRH. With this antenna pointing accuracy, it can be expected that phase errors in the visibility of short baselines used for calibration will amount to several degrees.

The work was financially supported by the Ministry of Science and Higher Education of the Russian Federation. SRH is the Large-Scale Research Facility “Radiogeliograph” of ISTP SB RAS [https://ckp-rf.ru/catalog/usu/4138190/].

REFERENCES

Altyntsev A.T., Lesovoi S.V., Globa M.V., et al. Multiwave Siberian Radioheliograph. *Sol.-Terr. Phys*. 2020, vol. 6, iss. 2, pp. 30–40. https://doi.org/10.12737/stp62202003.

Holleman I., Huuskonen A. Analytical formulas for refraction of radiowaves from exoatmospheric sources. *Radio Sci*. 2013, vol. 48, iss. 3, pp. 226–231. https://doi.org/10.1002/rds.20030.

de Vicente P., Barcia A. *Deconstructing a Pointing Model for the 40M OAN Radiotelescope (Technical Report)*. 2007, 25 p. URL: https://icts-yebes.oan.es/reports/doc/IT-OAN-2007-26.pdf (accessed February 17, 2026).

Mangum J.G. *ALMA Memo 366: A Telescope Pointing Algorithm for ALMA*. 2001, 21 p. URL: https://legacy.nrao.edu/alma/memos/html-memos/alma366/memo366.pdf (accessed February 17, 2026).

Perley R.A. High Dynamic Range imaging. *Synthesis Imaging in Radio Astronomy II. ASP Conference Ser*. 1999, vol. 180, p. 275.

Sun Zh., Wang J., Wang G. The establishment of pointing model for the Shanghai VGOS Radio Telescope. *J. Physics: Conference Ser*. 2019, vol. 1288, iss. 1, 012027. https://doi.org/10.1088/1742-6596/1288/1/012027.

Thompson A.R., Moran J.M, Swenson G.W., Jr. *Interferometry and Synthesis in Radio Astronomy*. 2nd ed. New York, Wiley, 2001, 692 p. https://doi.org/10.1002/9783527617845.

URL: https://ckp-rf.ru/catalog/usu/4138190/ (accessed February 17, 2026).

Original Russian version: Globa M.V., Gubin A.V., Lesovoi S.V., published in Solnechno-zemnaya fizika. 2026, vol. 12, no. 2, pp. 124–129. https://doi.org/10.12737/szf-122202613.

How to cite this article

Globa M.V., Gubin A.V., Lesovoi S.V. Correction for pointing errors of Siberian Radioheliograph antennas. *Sol.-Terr. Phys*. 2026, vol. 12, iss. 2, pp. 114–118. https://doi.org/10.12737/stp-121202613 .